Craniomaxillofacial Surgical Simulation and Planning

Graduate Research Paper

by

Cheng Yuan

under the guidance of

A/Prof. Leow Wee Kheng

SCHOOL OF COMPUTING

NATIONAL UNIVERSITY OF SINGAPORE

January 2010

Contents

Chapter 1

Introduction

1.1 Motivation

Facial deformities are distortions of some parts of the face of human. For example, there is one child born with cleft palate in 700 live births around the world [79] (Fig. 1.1) and one child born with facial asymmetry in every $5,600$ births [42] (Fig. 1.2). In addition, every year, more than 50 million people sustain car-related injuries, in which facial fracture is one of the most common injuries [76].

Craniomaxillofacial (CMF) surgeries are procedures that deal with the congenital and acquired deformities of the skull, jaws, nose, skin, muscle and teeth in the head and the face. They attempt to apply proper operations on the bones, teeth, muscles, blood vessels, nerves and skin of the patients to recover normal functions and appearance of the anatomical components. Therefore, CMF surgeries are very complex.

To help the surgeons perform precise and effective preparation for CMF surgeries, computer-aided surgical simulation systems for planning and simulation of CMF surgeries are needed. These systems should help the surgeons simulate various surgical operations, predict the surgical results of these operations, evaluate the effect of the surgical procedures and even determine the optimal surgical procedures.

Many surgical simulation systems have been developed for CMF surgeries [9, 10, 20, 24, 31, 35, 49, 67]. Some of the systems allow the users to practice and improve their operational

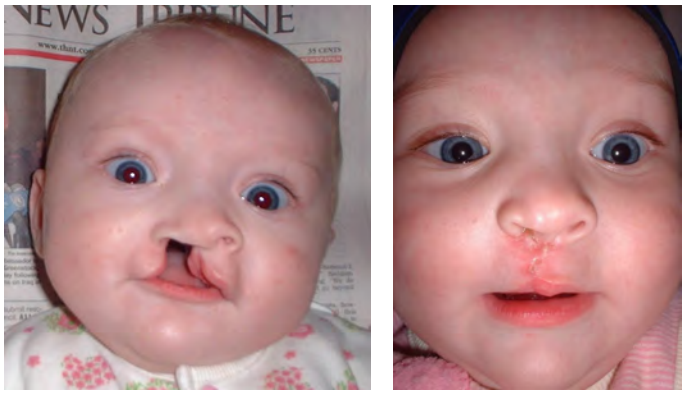

(a) (b)

Figure 1.1: Cleft palate refers to a separation of the parts or segments of the lip or roof of the mouth. (a) A six months children with cleft palate before surgery; (b) One month after the unilateral complete cleft lip repairing surgery [75].

skills at a low cost. The surgeons need to use the systems to sketch out their plans, and the systems produce the possible outcome to help them evaluate. Some systems help the surgeons on manipulating the bones [67]. Some other systems predict the deformation of the soft tissues to help the surgeon evaluate the resulting out appearance of the operations [9, 24, 31, 35]. Furthermore, a few systems have been developed to help the surgeons predict the implant shape [20]. Most of these systems have been evaluated or used in real application.

Many simulation systems have been developed for CMF surgeries. To start our research on surgical simulation of CMF surgeries, it is necessary to review state-of-the-art systems. The main purpose of this GRP is to review the existing surgical simulation systems especially for CMF surgeries, and find some topics worthy of further studying.

1.2 Related Topics

To do CMF surgical simulation, the first step is to acquire 3D computer anatomical models of a patient's head from medical images. 3D model building is a complex topic which consists of image segmentation and registration. After 3D computer model building, the next step is to determine the deformability of the model. With the deformability determined, it becomes possible for the systems to predict the outcome of a surgical operation.

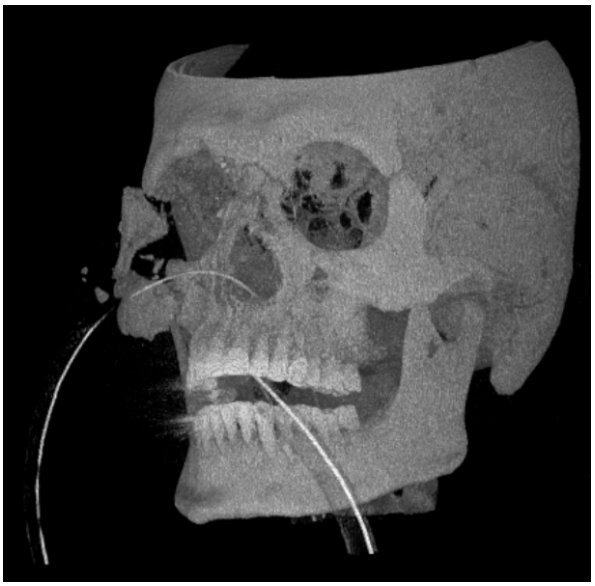

Figure 1.2: A patient with a fractured face after a accident.

Segmentation is to partition an image into several regions of interest. For examples, in CMF surgery, we need to segment the bones and the soft tissues from the medical images. In some specific cases the different types of soft tissues should further be segmented, too. The bones can be segmented by applying a threshold to the images, while the segmentation of the soft tissues should be done by more complex techniques.

Given two images of the same object, the registration problem finds the transformation to align them. Registration is necessary for surgical simulation systems. For example, the bone structures are more easy to segment in CT images, while the different types of soft tissues are more easy to segment in MR images. However, CT and MR images are taken by different equipment in different time. To utilize the segmented region of both CT and MR, it is necessary to align them. Therefore, the transformation between the two sets of medical images in different modes needs to be determined by registration.

The physical properties of different parts of the head should be modeled to simulate the deformation of them in response to surgical operations. On the one hand, the bones are rigid objects, their fracture and displacement should be modeled. On the other hand, the soft tissues are deformable objects whose properties should be carefully modeled to represent the real tissues. Thus, the physical properties of the materials should be properly modeled for prediction accuracy.

1.3 Organization

To understand CMF surgical simulation, it is necessary to introduce the medical background of the anatomy of the head and CMF surgeries (Chapter 2). Then, existing surgical simulation systems and algorithms are reviewed (Chapter 3). Based on the literature review, possible research topics are presented in Section 3.4. Preliminary work related to this research is given in Chapter 4. Chapter 5 concludes this paper.

Chapter 2

Anatomy of the Head

The head contains many components including blood vessels, lymph vessels, oral cavity, brain, nerves, nasal cavity, skin and skin appendages. CMF surgeries deal with bone, teeth, skin, muscle, nose and other soft tissues of the head. Therefore, in this paper, we limit our discussion of head anatomy on the bones, teeth, muscles, skin and fat.

2.1 Skull and Teeth

The skull's function is to protect the brain and support the facial structures (Fig. 2.1(a), Fig. 2.1(b)). The skull bones can be divided into two groups, the cranial bones (craniums) and the facial bones. The eight cranial bones are fused together, forming the cranial cavity which contains and protects the brain. The 14 facial bones form the mechanical framework of the face, providing the attaching sites for the muscles. The lower jaw, the mandible, is connected to the two temporal bones at the temporomandibular joints (Fig. 2.1(b), one on each side), which is the only two joints in the head that allow movement.

Humans usually have 20 milk teeth (Fig. 2.2(a)) and 32 permanent teeth (Fig. 2.2(b)). Teeth are usually classified as incisors, canines, and molars. Among the primary teeth, 10 are found in the upper jaw, the maxilla, and the other 10 in the lower jaw, the mandible. When people grow up, the primary teeth are replaced by permanent teeth. Among the permanent teeth, 16 are found in the maxilla and the other 16 in the mandible [36].

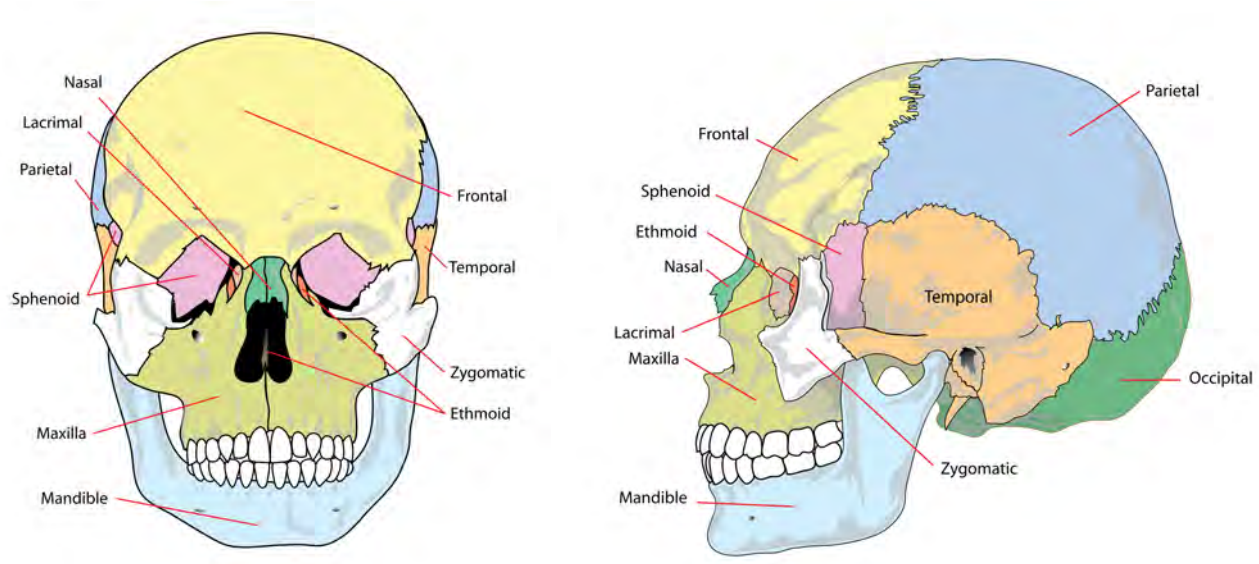

(a) (b)

Figure 2.1: (a) The frontal view of the skeletal and teeth structure of the head. (b) The side view of the skeletal and teeth structure of the head [74].

2.2 Muscles

The facial muscles in the head lie just under the skin and control facial expression (Fig. 2.3). They generally originate on bone, and insert on the skin of the face.

The mimetic muscles in different facial region have different functions. For example, the muscles in the prefrontal area control the eyebrow. The muscles around the eyes control closing, blinking and weeping of the eyes. Moreover, the muscles surrounding the nose can enlarge or reduce the size of the nostrils. Furthermore, the muscles around the mouth control the motion and shape of the mouth and the surrounding area. In addition, chewing muscles control the movement of the lower jaw during chewing and other activities, such as talking.

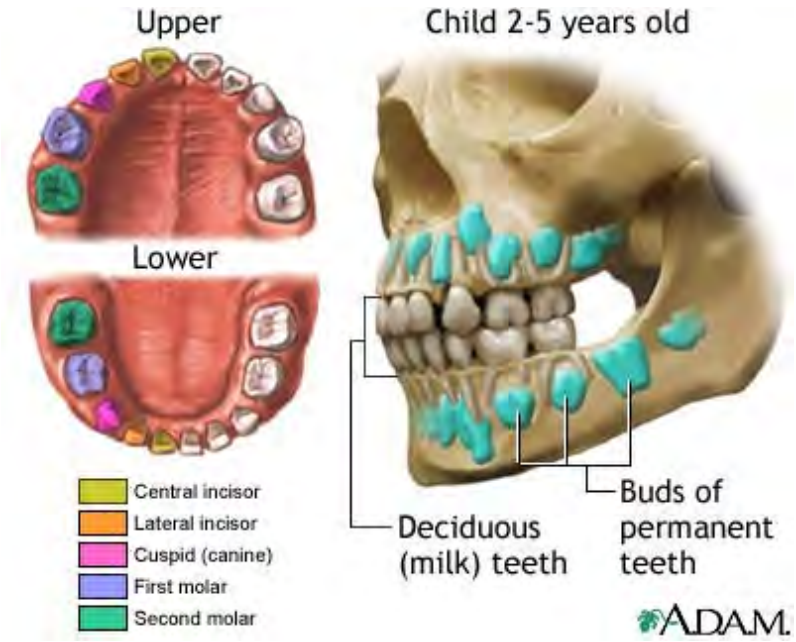

(a)

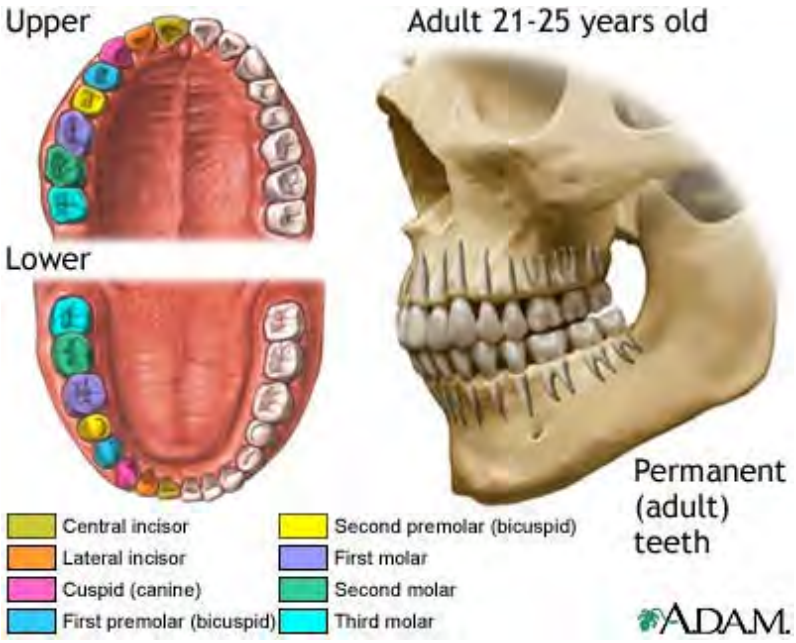

(b)

Figure 2.2: (a) The milk teeth. (b) The permanent teeth.

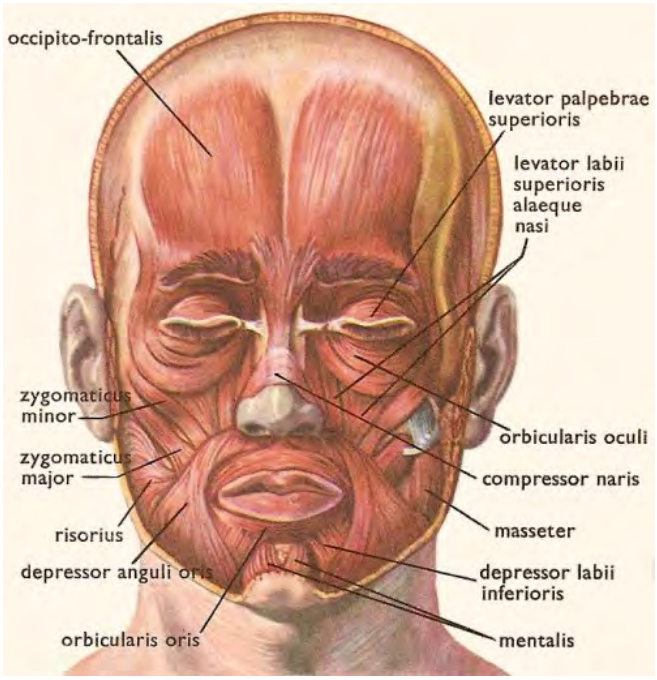

Figure 2.3: The facial muscles [56].

2.3 Skin and Fat

The facial skin is a soft covering of the internal systems. The skin is composed of three layers: epidermis, dermis, and hypodermis (Fig. 2.4). The epidermis layer is supported by the lower layers. The thickness of the epidermis layer is about 0.1 mm, so it has little influence on the elasticity of the skin. The inner layer is the dermis. Its thickness ranges from 0.6 mm to 3.5 mm, so the dermis determines the elastic property of the skin. The lowest layer of the skin is hypodermis which is 50% fat.

The main functions of the facial skin are protection of the internal systems, sensation of the external environment, storage of lipids and water, and heat regulation, etc. In the outermost layer, the epidermis serves as a protective barrier. In the middle layer, dermis, most of the skin appendages like hair, sweat gland and sensory nerves are located. In the inner most layer, the hypodermis loosely connect the skin to the underlying muscles and bones through connective tissue and elastin, allowing the skin to move.

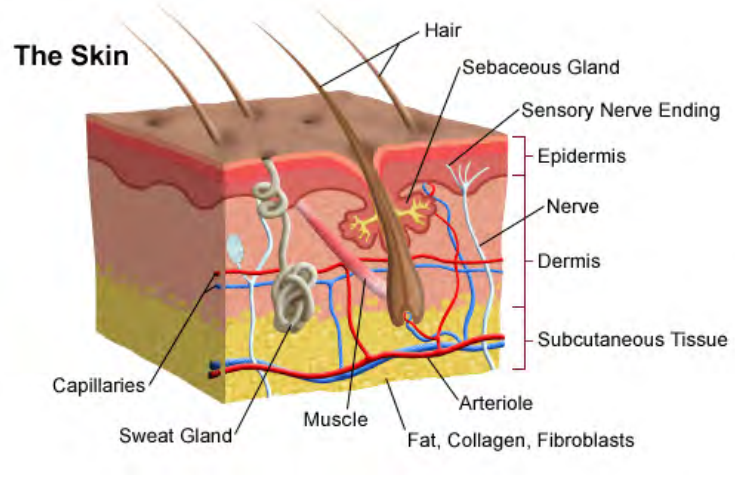

Figure 2.4: The skin anatomy [4].

2.4 Facial Appearance and Expression

Overall, there are three main components that contribute to the facial appearance. First, the skull and teeth form the supporting structure for the other components in the head. Second, the muscles are connected to the skull through tendons, which control the movement of the jaw and various facial appearance of a person. Finally, the skin is loosely connected to the muscles and bones through the hypodermis, and functions as the surface of the face.

The facial nerve controls the activation of the facial muscles. One or more movements of the facial muscles result in facial expressions. These movements convey the emotional state of the individual to the observers.

2.5 Conclusion

The CMF surgeries are mainly focused on operations of the head anatomies to recover the functions of the head components and build better facial appearance for the patients. There are two kinds of materials in the head influencing the appearance of a person. They are rigid parts (bones and teeth) and soft tissues (muscles, skin and fat, etc.) attached on them, whose physical properties are quite different.

Chapter 3

Literature Review

Many surgical simulation systems have been developed over the last decades [3, 37, 41, 70]. They can be divided in many ways. For example, based on interaction mode, they are divided into reactive systems and predictive systems. Based on the planning goal, they are divided into navigational planning, corrective planning and reconstructive planning. Furthermore, we discuss the deformation methods that can be used in these systems.

CMF surgical simulation systems covers only some of those categorizations. To better study existing surgical simulation systems, in each discussion, we will first discuss surgical simulation systems in general, followed by CMF surgical simulation systems.

3.1 Interaction Mode

From the way the surgical simulation systems interact with the operators, we can divide them into reactive systems and predictive systems according to their different characteristics.

Reactive surgical simulation systems [3, 26] attempt to give the users real-time reactions of the patient's body such as, displacement of body tissues, deformation of body tissues and bleeding, in response to surgical operations. These systems aim to provide the users with the perception of real surgical situation.

To predict the results of complex procedures, predictive systems are developed [19, 52, 67, 68]. They produce the surgical results based on a small amount of user inputs

indicating the key requirements. Thus, the surgeons can evaluate various surgical operations to determine the optimal ones to be applied on the patients.

3.1.1 Reactive Simulation Systems

Reactive surgical simulation systems give the user real-time response such as displacement of bones in response to the user inputs corresponding to the surgical operations such as incision, resection, opening and suturing. These systems aim to provide the users with the perception of real surgical situation. Thus, reality and interactivity are the most important objectives of these systems.

Reactive systems for needle-based procedures have been developed [26, 34]. These systems simulate body tissue deformation in response to needle insertions. Due to the simplicity of needle-based procedures, reactive systems can provide good visual and haptic feedback in real-time.

Reactive systems have also been developed for the simulation of minimally invasive surgeries (MIS) [21, 37]. MIS introduce specialized instruments into the body through small incisions, and use them to manipulate the body components. Visual feedback is obtained from the cameras attached to the inserted instruments. Constrained by the small entry portal, the instruments are usually designed to work in a limited range of motion. To improve the visual reality, a photo-realistic rendering algorithm that models the detailed reflectance of the mucous-covered surface is developed in [21]. Reactive systems for MIS simulate real-time soft-tissue deformation in response to the limited motion of the instruments, providing visual and/or haptic feedback to the user. In [37], a reactive simulation system called "Karlsruhe Endoscopic Surgery Trainer" is developed, providing simulation of several surgical operations like grasping, cutting, coagulation (which is used to destroy abnormal tissues or to form adhesive scars), injection, and suturing. This system provides visual feedback to the surgeons when they operate on the instrument box (Fig. 3.1). For more realistic simulation, the interface is designed as an artificial cavity together with the correct instrument set, which is very similar to the normal interface in physical simulation (Fig. 3.2).

Compared to needle-based procedures and minimally invasive surgeries, open surgeries have a larger visible field of more complex anatomy. In addition, the applicable motions of the surgeons are more complex in open surgeries. This makes the simulation of open surgeries

Figure 3.1: The instrument box for the surgeons to input surgical operations to the system [37].

Figure 3.2: The MIS training system for VR-based simulation of the cutting of the gall bladder [37].

more difficult [1]. As a result, most of the existing reactive systems for open surgeries are mainly focused on the simulation of simple basic surgical operations such as incision and soft tissue retraction [3, 62, 63], suturing of wounds [70], ventricular septal defect (a kind of heart defect) [62, 63] and bone drilling [33]. For example, a reactive simulation systems for simulating the removal of the bone behind the ear is developed in [33] (Fig. 3.3). It provides acoustic, visual and haptic feedback. This system simulates the real operative situation in three ways. First, pre-recorded audio samples for drilling, suction and irrigation are played when users perform the corresponding operation. Furthermore, to increase engagement, a fluid blood rendering is integrated into the bone rendering. Finally, a 3D hepatic device is used to produce force feedback.

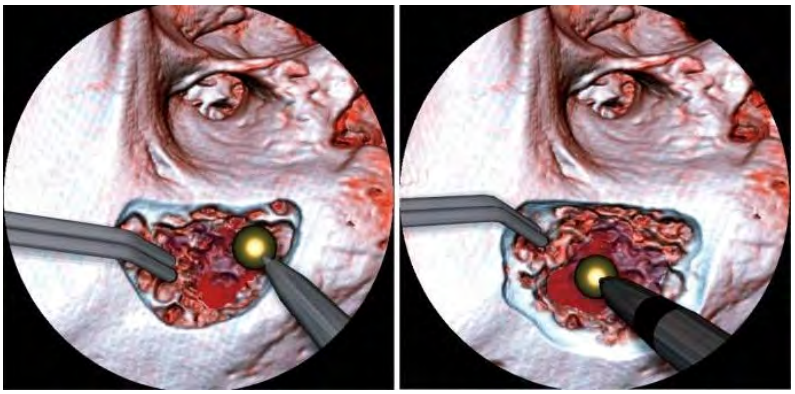

Figure 3.3: An example of reactive system for bone drilling, suction and irrigation [33].

3.1.2 Predictive Simulation Systems

Predictive surgical simulation systems produce possible surgical results based on a small amount of inputs given by the users. These systems only require the key operations of the surgeries, and do not come to the details of simulating the reactions of the body in response to the small operations. In contrast, predictive simulation systems directly give the resulted deformation of the anatomy after the surgery. By applying various surgical options in the predictive systems, the surgeon can easily access the simulation outcomes of the different options to select the optimal one. Thus, accuracy of the prediction becomes the most important objective for the predictive systems, while real-time response becomes less important.

Predictive systems have been developed for pre-operative planning of dental surgeries and surgical implants [19, 22, 64, 69]. They have also been developed for predicting post-operative alignment of bones in bone cutting [68] and surgical repositioning of fractured arm bones which are not properly fixed [52]. In these applications, the anatomical parts are all rigid objects such as bones and teeth.

For liver surgeries, systems for liver and tumor resection (i.e., cutting) plan are developed [6, 46]. Based on domain knowledge about the safety margins of the operations, they analyze segmentation results of CT images to propose the plan. The system in [46] also estimates the post-operative liver volume. For heart surgeries, a system developed in [39] can predict the result for surgeries involving cardiac blood vessels (Fig. 3.4). The surgeon only needs to indicate where to cut the blood vessel and where suture, and the system can

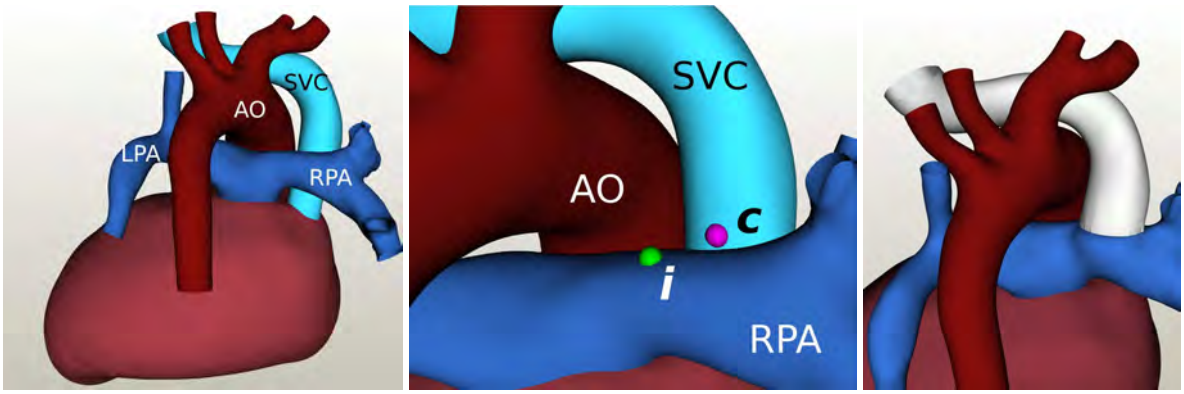

Figure 3.4: A predictive system for simulating surgeries on cardiac blood vessels [39]. (a) Heart and blood vessel models reconstructed from a patients CT images. (b) User input points to indicate surgical options. (c) Predicted surgical result.

predict the post-operative shapes of the blood vessels.

Some predictive systems are specially developed for the CMF surgeries [9, 10, 20, 24, 25, 29, 31, 32, 44, 67]. The systems developed in [44, 67] are for cutting bones and repositioning bones in CMF surgeries. Some systems have been developed for predicting external appearance due to cutting or displacement of bones [9, 24, 31, 32] and insertion of implants [20] (Fig. 3.5). Some other systems can predict the expressions of a person by simulating the activation of muscles [10, 25].

3.2 Planning Goals

There are three general kinds of surgery planning depending on the goal: navigational planning, corrective planing and reconstructive planning. Depending on how a surgery simulation system is designed, it may support one or more planning goals.

3.2.1 Navigational Planning

Navigational planning is concerned with planning for the optimal access to the body parts to be operated on. For example, in minimally invasive surgeries, a good selection of incision port and access path is important for shortening the operation time and reducing the risk to

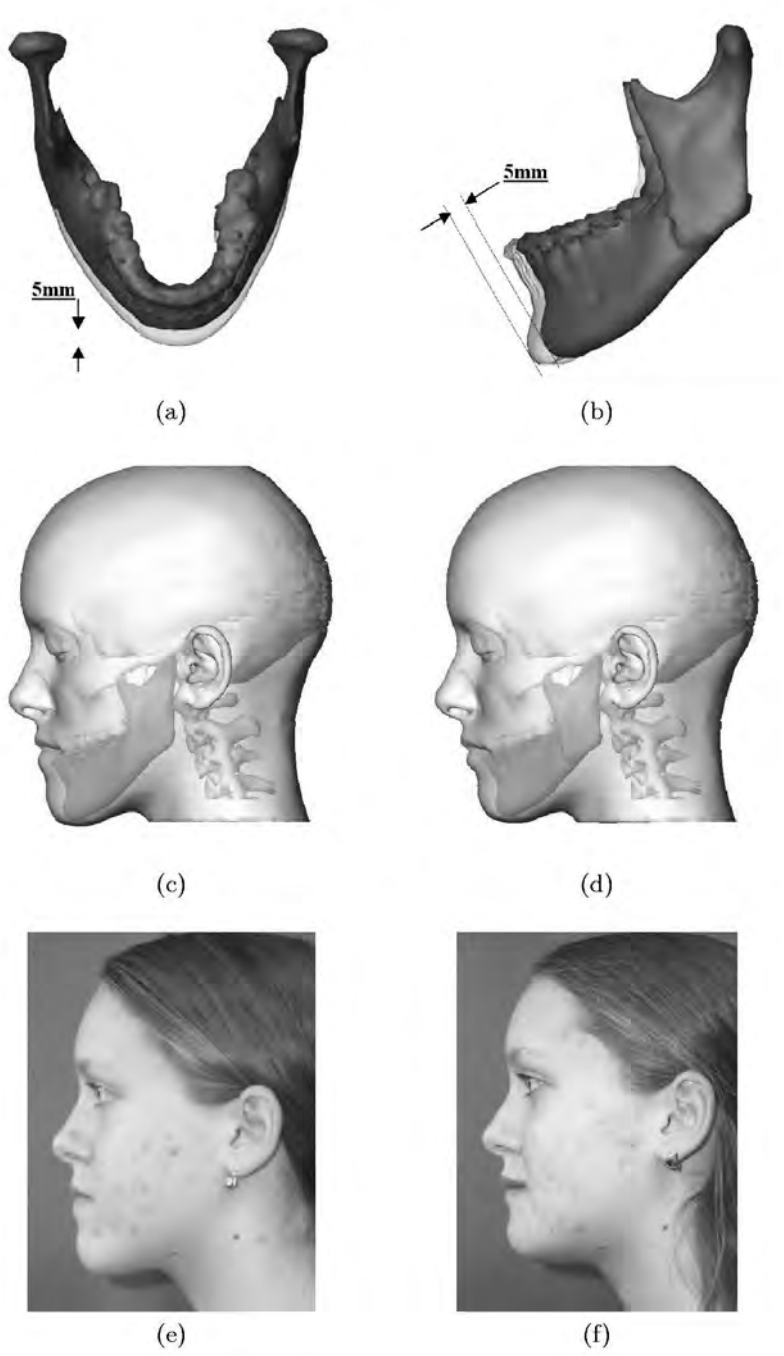

Figure 3.5: A predictive system for setting back the lower jaw. (a) and (b) The surgical operation. (c) Geometrical model of preoperative anatomy. (d) The result of the numerical soft tissue prediction. (e) Preoperative patient profile. (f) Postoperative patient profile. respectively) [20].

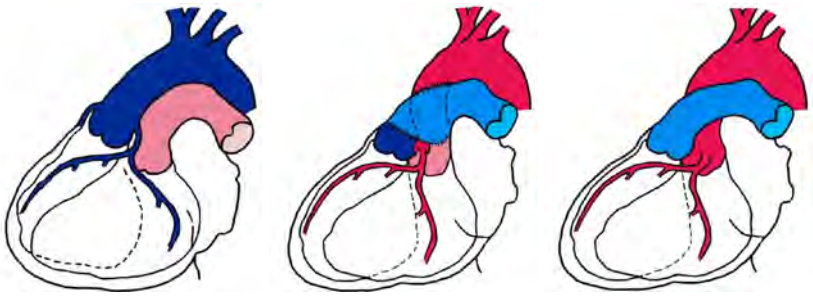

(a) (b) (c)

Figure 3.6: (a) Heart with transposition of the great arteries. (b) arterial switch operation. (c) Normal heart. From [40].

the patient. Navigational planning also provides surgeons with information about possible obstructions at and around the organs to be operated on.

A notable work of navigational system for heart MIS surgery is [12]. A static model of a patient is built by segmentation of the pre-operative CT images. This model is then used to automatically determine the optimal port location, depending on the target and entry chosen by the surgeon. In [73] the heart motion is taken into consider. The systems used 4D data (Time dependent 3D data) to calculate the optimal port location.

3.2.2 Corrective Planning

Corrective surgeries are the surgeries that correct malfunctioning body parts to restore proper function. For example, in transposition of the great arteries, a congenital heart defect (Fig. 3.6(a)), the aorta and the pulmonary artery of the patient arise from the wrong ventricles compared to a normal heart (Fig. 3.6(c)). For treating transposition of the great arteries, there is a corrective surgery called arterial switch operation (Fig. 3.6(b)). It disconnects the great arteries from their roots, switches them to reconstruct the neo-aorta and neo-pulmonary artery, and relocates the coronary arteries to the root of the neo-aorta [40]. From the figures, we can find that this corrective surgery is complex. Corrective planning plans the corrective surgeries needed to restore the proper function.

For heart surgeries, a surgical simulation systems in [39] is developed to assist the surgeons when they plan the bidirectional Glenn shunt (BDG) surgery. BDG is an operation

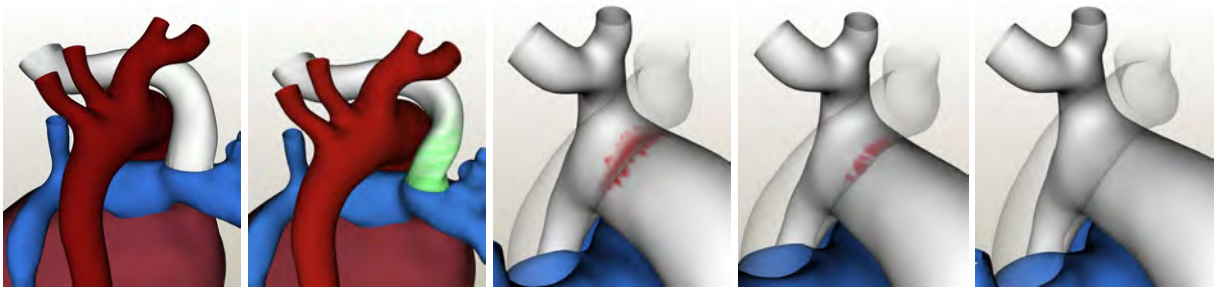

(a) (b) (c) (d) (e)

Figure 3.7: Predicted surgical results of various surgical options. (a) Optimal result, free of congestion and twisting. (b) Result with undesirable twisting indicated in green. (c to e) Different selections of cut points on SVC result in different amount of pressure due to collision with aorta. SVCs are made semi-transparent to illustrate the pressure in red [39].

that cuts the superior vena cava (SVC) and attaches it to an incision made on the top side of right pulmonary artery. In this system, the predicted shape of the blood vessels corresponding to different kinds of operations is visualized. This system helps the surgeons plan the corrective surgery by providing the predicted result to the surgeon when they change the operation. By evaluating various surgical procedures in the system, the surgeons can determine the optimal procedure to be applied (Fig. 3.7).

For CMF surgeries, many systems are designed to help the surgeons plan different kinds of corrective operations [9, 10, 20, 24, 25, 31, 32, 67]. For example, a system to calculate the post-operative appearance in response to the cutting, rotating and displacing of the mandible is developed in [9, 20, 24, 31, 32, 67]. This system helps the surgeon plan proper operations on the mandible, by evaluating many possible operations. Moreover, in [10, 25], systems for predicting the various facial expressions for the patient are developed. The surgeons can use these systems to plan a surgical procedure that corrects the most amount of the patients' abilities to facial emotion expression.

3.2.3 Reconstructive Planning

Reconstructive surgeries are surgeries that reconstruct the body parts that are damaged due to disease or trauma to restore their structures and functions. For example, the driver Rees-Jones suffered serious head injuries in the traffic accident that killed Diana, Princess of Wales.

His face was flattened: numerous bones were broken or crushed. His face was reconstructed from family photographs by a maxillofacial surgeon, Luc Chikhani, using about 150 pieces of titanium to hold the bones together and recreate the original shape [77]. Within a year, his face was nearly back to normal.

Up until now, only a few reconstructive systems for CMF surgeries are developed. One example is seen in [44], in which system visualize the bone model in 3D, and allow the surgeons to move the bone segments in the virtual reality. The planed repositioning of the bone segments is recorded. When the surgeons execute the surgery in the operation room the record is used as a guidance. Another example is a system for facial fractured recovery used in a team in National University Hospital, Singapore [29]. It uses the healthy part of a patient's facial bone to predict the appearance of the fractured part by lateral reflection.

3.3 Deformation Models

There are seven main types of deformable models: free-form deformation, mass spring model, finite element method, thin-shell method, differential geometry method, cosserat method and hybrid methods. Free-form deformation [62] deforms the 3D space that contains the object. The object is also deformed in this process. They are mainly used for 3D model building and computer animation. Free-form deformation methods do not work directly on geometric shape. It is difficult for them to explicitly manage geometric properties of the materials defined on meshes. Therefore, free-form deformation is difficult to be used in surgical simulation. For this, we will not expand our discussion to free-form deformation approaches.

3.3.1 Mass Spring Model

MSM is a network of mass points connected by massless springs [37]. When external forces act on the system, the deformation of the springs would generate forces opposite to them. The state of MSM model at a given time is defined by the positions and velocities of the mass points. The velocities of points are determined by the forces added on them based on Newton's law. Numerical solution of mass spring equation is solved to find the stable positions of all mass points, which determine the deformation of the object in response to

the external forces.

The implementation of MSM is simple compared to other methods. In addition, MSM is computationally efficient. Thus, MSM can be fairly large and complex without compromising real-time response [38]. Therefore, MSM is widely used for real-time surgical simulators, in which efficiency is the most important criterion.

A prostate model is built in mass-spring style in [8]. This model can reactively simulate resection and deformation of the prostate and tissue in a MIS to remove the prostate tissue that obstructs the unary flow. MSM is used in [11] to support simulation of interactive cutting on deformable anatomy. In [41], MSM was used for a visual and haptic simulation of progressive suturing. MSM is applied in [37] to develop a system for MIS (Fig. 3.2). For heart surgery, a system in [50] applied a MSM called LR-spring mass model, which combines *L*ocal interaction [7] and iterative *R*elaxation [15], for real-time simulation. Later, GPU is utilized in their system to accelerate the simulation [51].

For CMF surgery, a three-layer MSM is used in [32] to simulate the facial external appearance due to bone realignment. The three layers and the springs between them are used to represent the physical properties of the three layers of the skin. In [66], MSM is used to build a system for interactive simulation of the bone cutting and soft tissue changes caused by bone movement. A fast version of the mass spring model is given in [48] and embedded into the simulation system to calculate soft tissue deformation in response to bone movement [49]. This model only calculates the external forces of the points who have at least a neighbor who has moved in the last iteration. If the external force to a mass point is less than some value, its movement is not considered.

MSM is computationally efficient and easy to implement, but it has several drawbacks. Simulation using MSM is not very realistic. The structure and resolution of the model have significant influence on the performance of the systems. Currently, there is no standard structure for different anatomies and operations. A genetic algorithm is used by [2] to build up the mesh topology of MSM. The problem for this approach is that it requires a reference model, which is unavailable in most of the practical situations. In addition, the biomechanical behavior of soft tissue is complex and inhomogeneous. The precise setting of the spring constants of different parts of the whole model is a challenging problem.

Numerical integration methods for solving MSM equations are not always stable. The stability of the solution depends on the time step and the integration scheme [53]. The

general condition for numerical stability is that the time step should be small. An analysis of the stability conditions for different numerical methods is given in [28].

3.3.2 Finite Element Method

FEM formulates soft tissue deformation in a continuous domain. In FEM, the deformable object is considered to be a continuous volume. The continuous volume is discretized into elements using an irregular mesh. The deformation of the object is represented by an energy function derived from the external forces and the internal energy defined by stress and strain. The object reaches its equilibrium shape when its potential energy reaches a minimum.

There are some advantages of FEM compared to MSM. The first advantage is that the biomechanical parameters of the tissues can be directly mapped to the parameters of FEM. In addition, FEM gives a more accurate and realistic modeling of soft tissue deformation than MSM.

In surgical simulation, there are many applications that use FEM to simulate deformation. FEM is used in [14] to predict the post-operative out-come for cataract surgery. The cornea deformation resulting from the muscle forces and intra-ocular pressure were simulated. FEM is also used to simulate the response of aorta during blunt traumatic impacts [60]. It included a thorax and heart model that simulated the response of the heart following a thoracic impact. FEM is applied in [78] to analyze left ventricular wall stress in patients with severe cardiac disease.

In the simulation of CMF surgeries, the problem of predicting the appearance of the face in response to bone displacement and the problem of predicting the shape of the bone implant for a desired appearance are formulated in [20]. By solving the problem in FEM [24], this system can predict the facial external appearance in response to bone movement, as well as the shape of the implant needed to achieve a certain external appearance. In [10], a manually generated hexahedral finite element model of the face, skin and muscles is registered to the patient specific data to build the patient specific model for simulation.

FEM has some drawbacks compared to MSM. The major one is the high computational complexity of FEM. An empirical comparison between MSM and FEM is provided in [31]. Firstly, A layered mass spring model is built to model the different properties of the layers of the real skin. Then MSM is used to simulate the external appearance in response to cutting

and displacement of the bones. At the same time, a FEM method is also built and applied on the same test case. The result shows that FEM is about 10 times slower than MSM.

Some algorithms are designed to reduce the computational complexity of FEM. A way is to reduce the number of elements using an adaptive coarse-to-fine model, which is complex in regions with large gradients and simple in quiescent regions [13, 80]. In [54, 55], an iterative algorithm for an interactive simulation of cutting is presented. These methods trade model accuracy for processing speed.

3.3.3 Thin-shell Model

Thin-shell model is used to model structures like shell and plate whose thickness is negligible. An introduction to this method can be found in a survey on surface deformation models [5]. Thin-shell models are based on a physically accurate representation of the materials. First fundamental form [18] measures length and area on the model. The change of first fundamental form corresponds to the surface local change in length and measures stretching. Second fundamental form [18] measures curvature on the model. The change of second fundamental form corresponds to the change of surface curvature and measures bending [65]. The minimization of the elastic energy function with boundary constraints is required to solve for the equilibrium state of the deformation process.

The minimization of nonlinear energy function in physically accurate formulation is expensive. Therefore, a simplified energy representation is used in [23, 71]. Then the problem is reduced to a linear minimization problem. Furthermore, the model is discretized into a triangular mesh [27]. Spring energy and change of dihedral angle in the mesh is used to approximate the stretching and bending energies.

Thin-shell model is more efficient for simulating objects with small thickness, compared to FEM, which has to use high resolution for accurate simulation. On the other hand, thin-shell model is physically more accurate than mass spring model. This is because the bending and stretching energies in thin-shell model emulates the real potential energies of thin objects. Thin-shell model has been applied to corneal surgical simulation to evaluate the post-operative result of corneal operations [30].

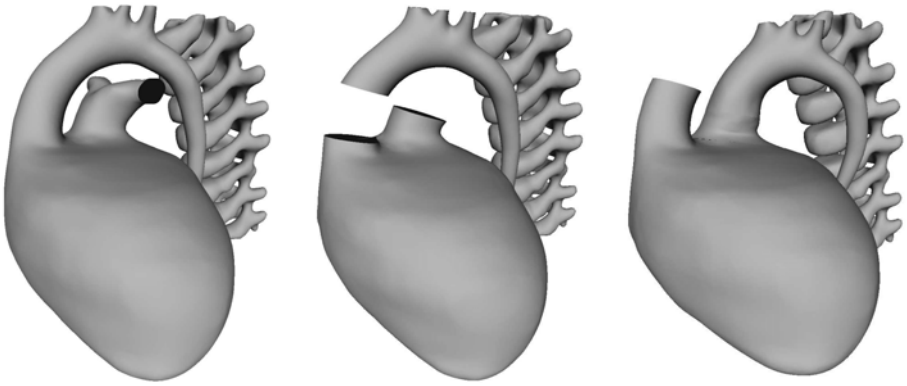

Figure 3.8: A DG method is introduced to surgical simulation by [40] to simulate the transaction of the aorta and pulmonary trunk in hear surgery. (a) before surgery. (b) the transection process. (c) the predicted surgical result.

3.3.4 Differential Geometry Method

Differential Geometry (DG) method, which is also known as partial differential equation (PDE) method in [45], directly solves for the positions of the mesh points after deformation, given the initial configuration of the object and predefined constrains on the geometric properties of the mesh surface. A linear or non-linear solver is used to solve the system equations, depending on the constrains.

An example of DG method can be found in [45]. The DG method in [45] introduces soft constrains for preserving the mean curvature normals. With other additional hard constrains modeling the operations on the mesh model, a least square system is constructed. By solving the least square system using QR decomposition, the stable position of the mesh points are determined. A DG method similar to the one in [45], is used to surgical simulation for heart surgeries by [40] (Fig. 3.8).

Another DG method is to model the mesh surfaces using Poisson method [59], which describes the differential properties of mesh surfaces in terms of continuous partial differential equation. It can, therefore, model smoothness and continuity naturally. However, the requirement that the boundary conditions on all boundaries is known could not be met in many practical applications.

DG is easy to implement and is relatively fast compared to FEM and thin-shell model.

For 3D meshes, DG method achieves near real-time deformation [45]. For 2D meshes DG method achieves real-time deformation [72]. However, it is unlikely to use DG method in reactive systems. DG does not explicitly model external physical forces acting on the object. It directly predicts the new stable state of the object in response to the external forces. Thus, it is not likely for DG method to simulate the intermediate state of the convergence of the model in response to the user operations.

For predictive systems, which do not need to simulate the intermediate transformation of the tissues, DG methods can be helpful. Though various geometric constraints can be incorporated into the deformation scheme, it is still a challenging task to translate elastic properties of materials to geometric properties of the mesh.

3.3.5 Cosserat Rod

Surgical simulation systems often encounter the simulation of tubular objects like catheters, sutures and blood vessels. The FEM and thin-shell models can model these objects. However, they are in general computationally expensive and they do not explicitly model global bending and twisting of the tubular objects.

Cosserat rod model (Fig. 3.9) was first introduced to the computer graphics community in [57]. In Cosserat rod model, the linear strain and the angular strain of each segment of the rod and the corresponding potential energy of the whole rod can be calculated. The positions of the rod segments are determined by minimizing the potential energy given the boundary constrains. It is shown that models based on the Cosserat theory of elastic rods are well suited for interactive simulation of tubular objects.

There is an assumption in Cosserat rod theory that the rod has rigid cross-sections that are small compared to its length. Therefore, most of the existing methods using Cosserat rod only apply to simulation of thin rods with small and rigid cross-sections. These conditions are not valid for blood vessels, which are hollow tubes with large and deformable cross-sections. A hybrid model that combines a Cosserat rod and DG mesh is developed in [39], which we will discuss in the next section.

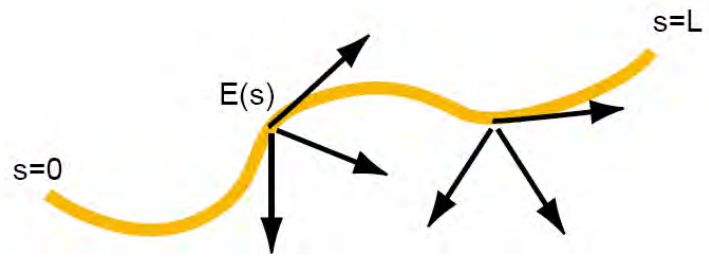

Figure 3.9: The Cosserat rod model. Each material segment is associated with three vectors: one is to represent the direction of the cross-section, the other two are used to represent the rotation in the cross-section plane [57].

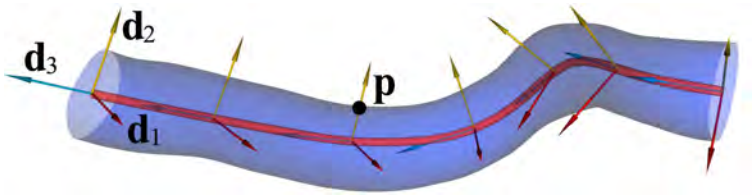

Figure 3.10: A hybrid model for blood vessel composed of Cosserat Rod and surface mesh used in [39].

3.3.6 Hybrid Models

Some researchers apply hybrid models that combine two or more other deformation models. These hybrid models take advantage of all the models in them. Therefore, it is possible for them to perform better than the individual models.

A successful example of hybrid model is developed in [39] for modeling blood vessel in heart surgeries. The model for the blood vessel is composed of a reference Cosserat rod and a surface mesh elastically attached to it (Fig. 3.10). The reference rod models the physical properties of the blood vessel, which ensures that the blood vessel deforms in a physically correct manner. The mesh models the details of the blood vessel surface. In this way, accurate and efficient deformation of blood vessel is achieved.

A proper hybrid use of different deformation models can achieve better performance than the individual models. Therefore, for CMF surgical simulation, a hybrid model might also be helpful.

3.3.7 Summary

Each of six deformation models discussed has its advantages and drawbacks. First, simplicity and efficiency are the advantages of MSM, but MSM cannot ensure realistic and stable simulation. Second, FEM can achieve more realistic simulation than MSM, but the computational complexity constraints its applications that do not require fast response. In addition, the thin-shell and DG model are more efficient than FEM, and more accurate than MSM. However, it is difficult to use geometrical properties of the DG mesh to represent the physical properties of the materials. Cosserat rod model is physically correct and efficient. Its limitation is the assumption about the small and rigid cross-sections of the rod. Finally, hybrid models that combine several models can take advantage of individual models.

3.4 Conclusion and Possible Research Topics

Most of the surgical simulation systems for CMF surgeries are predictive systems predicting the post-operative appearance of the patient in response to the surgeons operations. Few interactive systems has been developed for the CMF, which is a kind of complex surgeries. Furthermore, most of the CMF surgical simulation systems are designed for corrective purpose [9, 10, 20, 24, 25, 31, 32, 67]. Only a few reconstructive systems are developed for CMF [29, 44]. Navigational systems are also developed to assist the surgeons shorten the operation time and reduce the risk. Not much attention has been paid on surgical simulation systems for reconstructive CMF surgeries like fractured face recovery surgeries.

Based on these observations, we found some topics on surgical simulation of CMF surgeries are still not well treated and worthy of exploring.

3.4.1 Reconstructive Surgical Planning of CMF Surgeries

From Table. 3.1, we know that few surgical simulation systems have been developed for reconstructive CMF surgeries. In fact, there are some interesting topics related to surgical simulation for reconstructive CMF surgeries. Take fractured face recovery surgery for example. The surgical objective is to recover the normal functions and structure of the face. One interesting problem for the surgical simulation systems might be how to help the surgeons

Table 3.1: Categorization of existing surgical simulation systems according to interaction mode and planning goal.

	Reactive	Predictive
Navigational planning	_____	Heart surgery [12, 73].
Corrective planning	MIS [37]. Heart surgery [26, 50, 51, 61, 62, 63]. Prostate operations [8].	Bone movement [52, 67, 68]. Dental surgery [19, 22, 64, 69]. Heart surgery [39, 40, 78]. CMF [9, 10, 20, 25, 31, 32, 48, 49, 66]. Cornea surgery [14, 30].
Reconstruction	MIS [44].	CMF surgeries [29].

determine the normal anatomy of the patient based on the normal photos and the 3D data of the fractured anatomy. In addition, automatic bone fracture detection is helpful for the surgeons, which might be another topic worthy studying.

3.4.2 Hybrid Modeling of Soft Tissues in CMF Surgical Simulation

As illustrated in Table. 3.2, most of the surgical simulation systems for CMF surgeries are using MSM or FEM methods. In the systems using MSM methods, the accuracy and stability can not be guaranteed. In the systems using FEM methods, the efficiency is low. It is hard to avoid these intrinsic drawbacks in these systems. From [39], we found that the hybrid use of DG method and Cosserat rod model have achieved high accuracy and efficiency of BDG simulation. Therefore, to design a proper hybrid model specially for head structures has potential benefits of improving the accuracy and efficiency of the CMF surgical simulation.

Table 3.2: Categorization of existing surgical simulation systems in terms of interaction mode and deformation method.

	Reactive	Predictive
Rigid Model	_____	Bone alignment [29, 44, 52, 67, 68]. Dental surgeries [19, 22, 64, 69].
Mass Spring Model	Basic surgical operations [3, 11, 41, 70]. MIS [37]. Heart surgery [50, 51, 62, 63]. Prostate operations [8].	CMF surgery [12, 31, 32, 48, 49, 66, 73].
Finite Element Method	Basic surgical operations [54, 55]. Needle-based surgeries [26]. MIS [61].	Heart surgery [78]. CMF surgery [9, 10, 20, 25, 31]. Cornea surgery [14].
Thin-shell Model	_____	Cornea surgery [30].
Differential Geometry Method	_____	Heart surgery [40].
Cosserat Rod Model	Needle-based operations [57].	_____
Hybrid Model	_____	Heart surgery [39].

Chapter 4

Preliminary Work

4.1 Facial Bone Segmentation

In CMF surgery, we need to segment the bones and the soft tissues from the medical images. The bones can be segmented by applying a threshold to the images. As a start up of this research, we implemented the threholding segmentation algorithm for head bones.

4.1.1 Input

Bone is very differetiable in CT images. Thus, the input of the thresholding segmentation algorithm is a series of CT images of the patient's head. These 2D slices are stacked to form a 3D volume data for the patient. The voxel value of the volume data ranges from 0 to 4095 for most of the data in our database. Let's denote the i'th voxel as x_i and the voxel value of the x_i as $V(x_i)$ A rendered picture showing a volume data for a patient is shown in Fig. 4.1. An open source software ParaView [58] is used for volume rendering of the data.

4.1.2 Output

The desired output of the segmentation algorithm is the labels for all the voxels in the volume indicating the the foreground-background properties. Note these labels as $L()$, which is a function of the voxel (if voxel x_i is a voxel belonging to the object of interest, $L(x_i) = 1$,

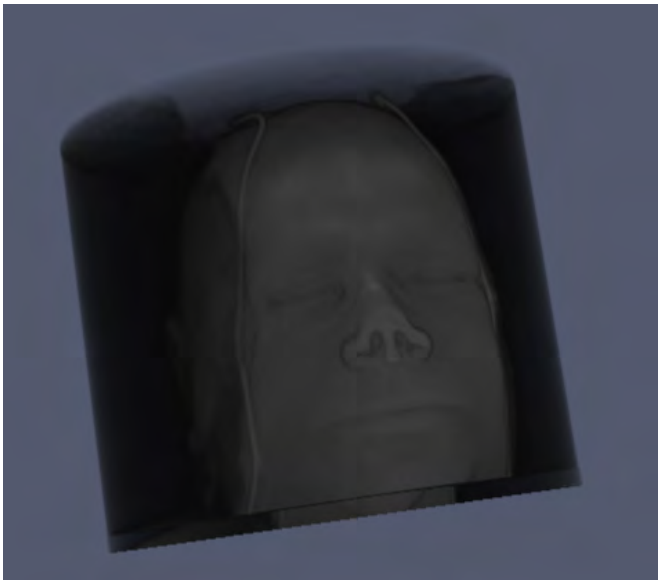

Figure 4.1: An example of the input of the segmentation algorithm.

otherwise $L(x_i) = 0$).

4.1.3 Method

A predefined threshold T is used in thresholding segmentation algorithm. For each voxel x_i in the volume, compare its voxel value $V(x_i)$ with T. If $V(x_i) > T$, then $L(x_i) = 1$ (classify x_i as a point of the object of interest); otherwise, $L(x_i) = 0$ (classify as background).

4.1.4 Experimental Results

The algorithm is applied on some CT data to determine the parameter (T) of the algorithm as well as evaluate the performance. The results show that for the bone segmentation of our test CT data, the threshold $T = 1150$ works very well (Fig. 4.2). After thresholding, a mesh building algorithm called marching cubes [43] can be applied to build a 3D mesh model of the skull (Fig. 4.3).

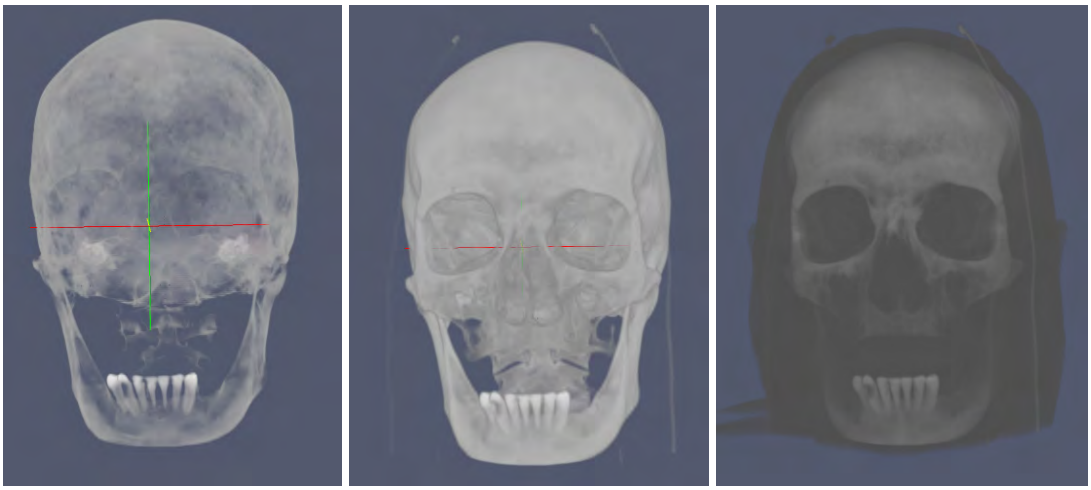

(a) $T = 2208$ (b) $T = 1150$ (c) $T = 736$

Figure 4.2: The different segmentation result for differet T. The background voxels are set to be fully transparant when rendering.

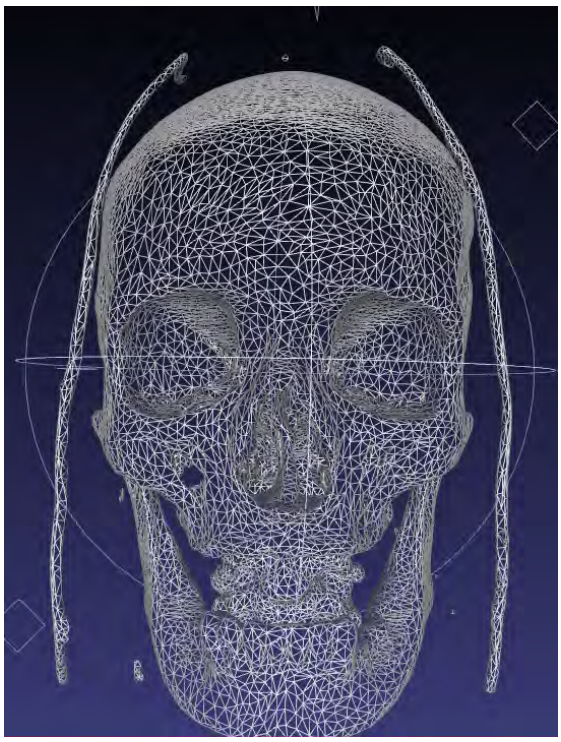

Figure 4.3: A 3D mesh model for the skull is built by marching cubes algorithm after thresholding segmentation. An open source software Meshlab [47] is used to render the 3D mesh model.

4.1.5 Conclusion

This work shows that for the segmentation of bones in the head CT. The thresholding segmentation algorithm works very well. The result of this work is important for the model building of the simulation system. As a future work, an appropriate algorithm for facial tissues segmentation should be implemented.

4.2 Salient View Point Selection

To develop a user friendly system for surgical simulation, we have developed an algorithm to find the salient viewpoint for a given volume date of the patient. This algorithm can find the salient viewpoint for a volume data based on the saliency defined as a combination of mean gradient and the entropy of the scene.

Currently, this work is used in finding the salient view point for medical volume image summarization [17]. After segmentation, the whole image is volume rendered and the viewing angle that reveals the most amount of information is automatically determined. As referred in Chapter 3, we planned to develop a bone fracture detection algorithm for CMF surgeries. When the fracture detection algorithm is done, it will be integrated into this work to achieve fracture based salient view selection, which would automatically detect the fracture parts from the volume data of the patients and automatically exhibit them to the surgeon.

Before salient view selection, the objets of interest is segmented by a soft segmentation algorithm proposed by a senior student in our group [16]. In this algorithm, the users only need to some simple markup work, the algorithm can find the opacity value for each voxel of the volume data indicating the foreground and background objects. We do not come to the detail of the implementation of the segmentation algorithm in this paper.

4.2.1 Formulation

Finding the salient viewing angle by rotating the camera with respect to the volume image I is equivalent to fixing the camera while rotating I. The centroid of I is aligned with the camera's optical axis, and the scale is normalized so that the projected 2D image of I has a fixed size. Rotation of I with respect to its centroid is represented as $\Theta = \{\theta_1, \theta_2, \theta_3\}$.

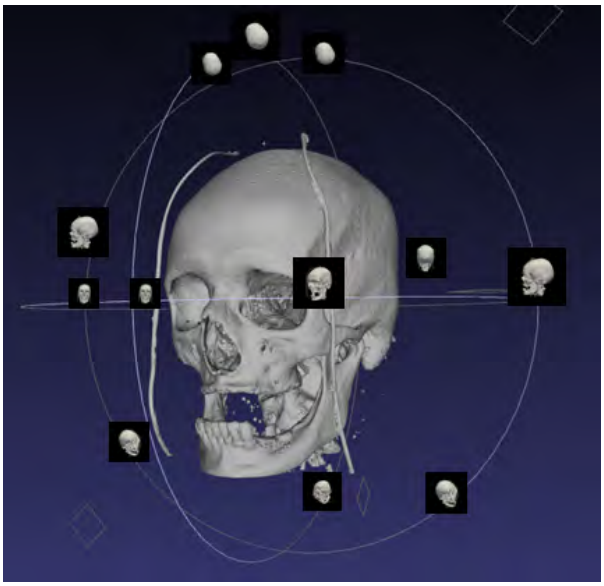

Figure 4.4: The segmented object of interest and the different views can be seen from different view point

In-plane (image) rotation θ_3 is set to 0 since it has no effect on the saliency measure of the projected image. Therefore, the problem is to find the out-of-plane rotation θ_1 and θ_2 that maximize saliency.

Given object rotation Θ, denote the projected 2D image of I as $J(\Theta)$. The saliency M of J consists of two terms,

$$M(J) = E(J) + wG(J) \tag{4.1}$$

where w is the weighting coefficient that balances the entropy $E(J)$ and the average gradient magnitude $G(J)$, which are defined as

$$E(J) = \sum_i -p_i \log_2 p_i, \tag{4.2}$$

$$G(J) = \frac{1}{N} \sum_x |\nabla J(x)|, \tag{4.3}$$

with p_i the probability of intensity i, and N the number of pixels in the projected

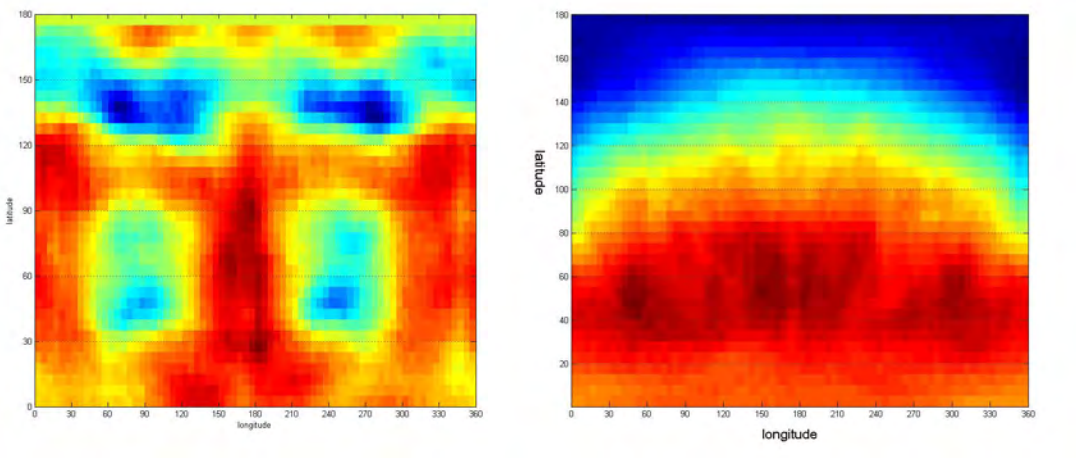

(a) Entropy (b) Gradient

Figure 4.5: The distribution of entropy and gradient with respect to θ_1 (longitude) and $theta_2$ (latitude) of Θ for the skull case

image J. The entropy term $E(J)$ measures the local variation of intensity values in a view (Fig. 4.5(a)). It is large when the view shows the part of the volume that is rich in both large-scaled surface features such as edges and ridges, and small-scaled surface features such as corners and saddle points. However, noise can be confused for small-scaled surface features. The average gradient magnitude $G(J)$ measures the global variation of intensity values in a view (Fig. 4.5(b)). It is large when the view shows the part of the volume that is rich in large-scaled surface features, and it is more resilient to noise than $E(J)$. By combining $E(J)$ and $G(J)$, their individual weakness can be mitigated. Therefore, the combined measure $M(J)$ facilitates the detection of salient view that is rich in 3D surface features while remaining resilient to noise (Fig. 4.6). Analogous entropy and gradient measures have been used in existing work for the determination of salient views for 3D mesh models.

4.2.2 Algorithm

The orientation that maximizes saliency M is determined by using an iterative maximization algorithm that is analogous to gradient ascent:

Repeat for a fixed number of iterations:
1. Randomly initialize Θ, and set the size of neighborhood δ to an initial fixed constant.

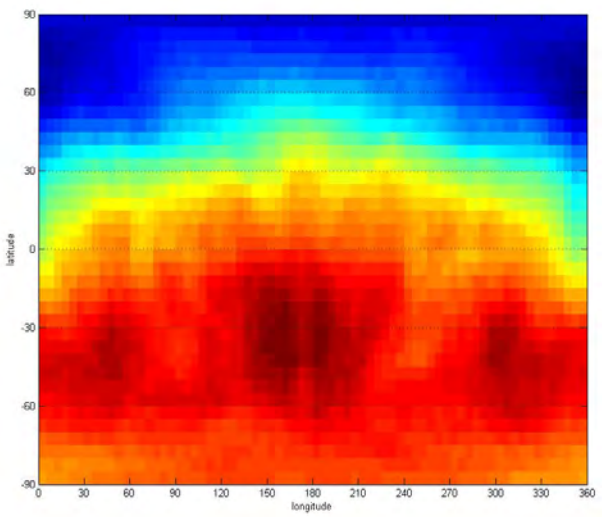

Figure 4.6: The saliency distribution for the skull case

2. Repeat until δ is small enough:
   a. Find the neighbor Θ' of Θ with the largest saliency.
   b. If $M(J(\Theta')) > M(J(\Theta))$, set $\Theta \leftarrow \Theta'$; otherwise, reduce δ.

The neighbors of $\Theta = (\theta_1, \theta_2, 0)$ are $\Theta' = (\theta_1 \pm \delta, \theta_2 \pm \delta, 0)$ (Fig. 4.7). The algorithm iteratively determines the angle Θ that maximizes the saliency $M(J)$.

After running this algorithm, we get a satisfying result for the example case (Fig. 4.8).

4.2.3 Experimental Results

To do more evaluation on the visual clarity of our selected views, we compare them with single 2D slice, conventional volume rendering, and possible sub-optimal views. Tests were conducted on medical volume images to evaluate the effectiveness of the proposed algorithm and its applicability to different types of images. The input volume images include head CT, abdominal CT, heart CT, and brain MR images, each containing 120–360 slices of resolution 512×512. The objects of interest range from hard objects like bones to soft tissues such as heart, liver, blood vessels etc. Only a selected set of comparison results are presented in this paper.

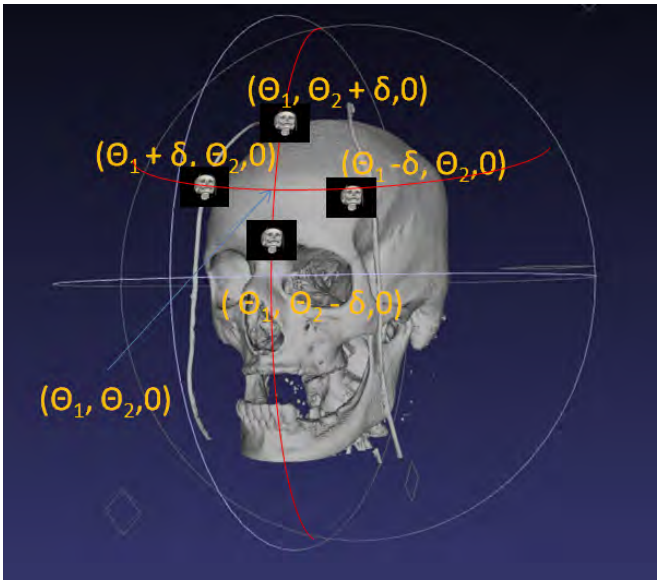

Figure 4.7: The neigbhors of $\Theta = (\theta_1, \theta_2, 0)$

Figure 4.9 shows the selected examples of the summarization tests. These objects have significantly different anatomical structures. Our results shown in Fig. 4.9(c) present very informative views about the objects, compared to visualization by a single 2D slice (Fig. 4.9(a)) and by conventional volume rendering (Fig. 4.9(b)).

Summarized images from sub-optimal viewing angles are demonstrated in Fig. 4.9(d). They either reveal less shape information about the objects of interest compared to those with salient viewing angles (skull and liver), or cause self-occlusions (multiple organs, hepatic vein and bronchi). These results show that our algorithm can indeed determine salient viewing angles.

4.2.4 Conclusion

In this work, we have developed an algorithm to find promising views for a given volume data. Compared with the convetional default view of the volume data and sub-optimal views, the views found by our algorithm reveal much more information of the data. The future work may be developing a fracture detection algorithm and integrating it with this salient view determination algorithm (Fig. 4.10).

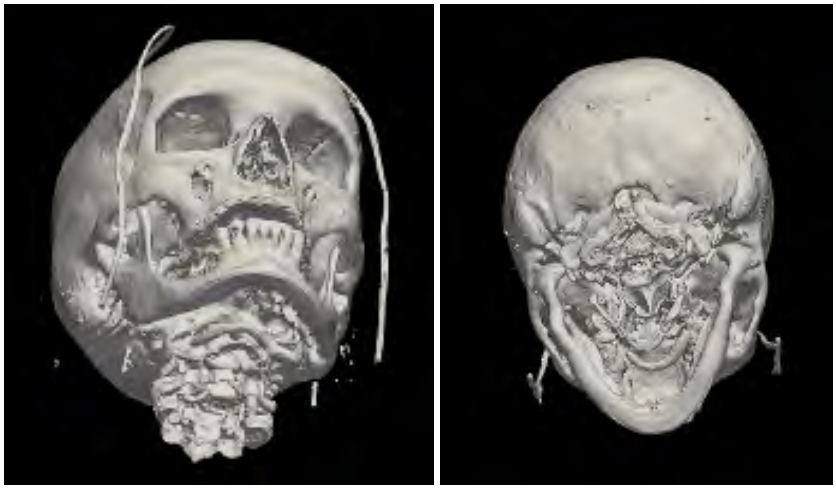

(a) Our result (b) Sub-optimal result

Figure 4.8: Comparism between the salient view found by our algorithm (a) and the possible sub-optimal view (b)

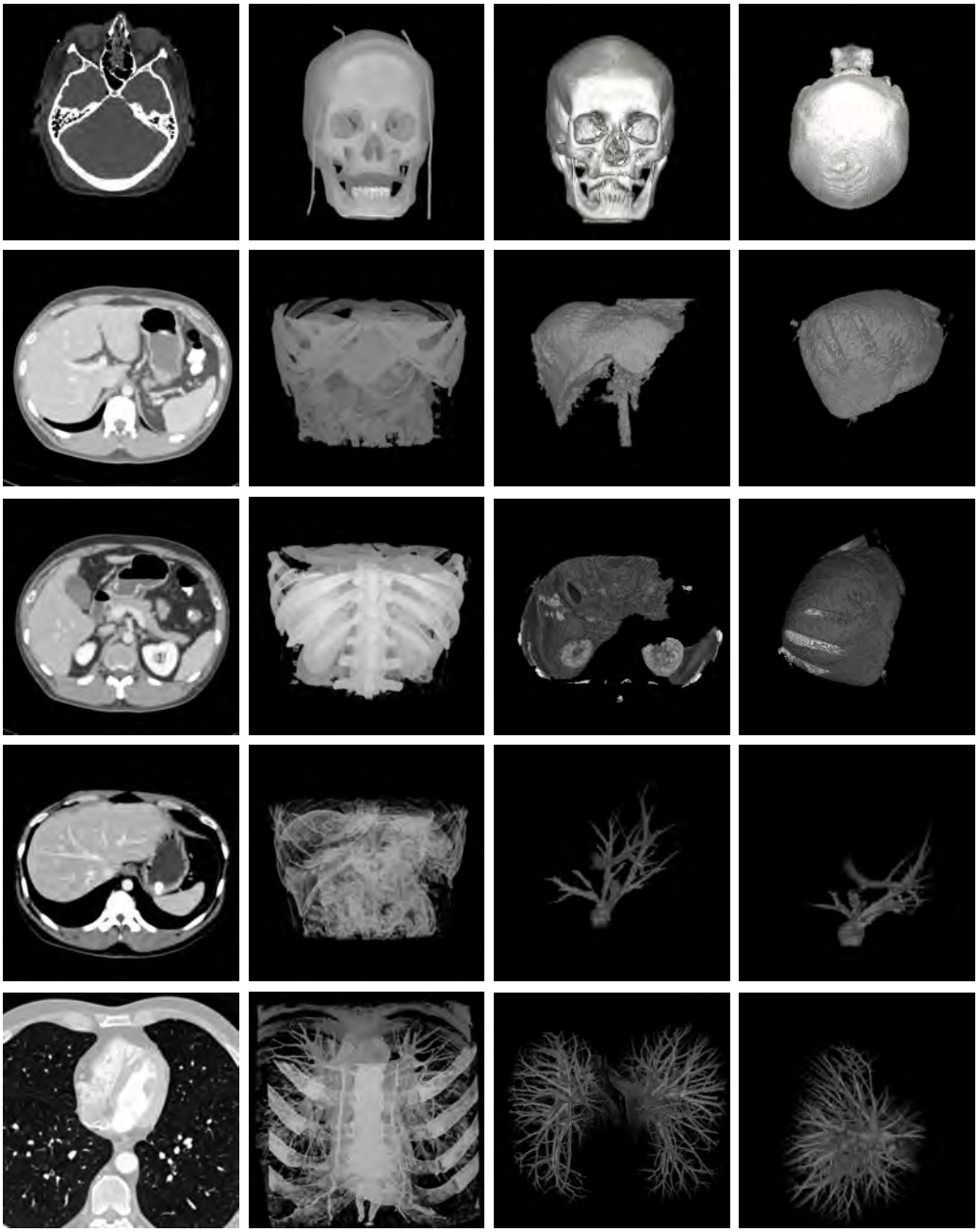

Figure 4.9: Summarization results of volume images. First row to last row: skull, liver, multiple organs, hepaticvein and bronchi. (a) Single 2D slice. (b) volume rendering. (c) Proposed algorithm: segmentation and salient view selection and (d) other sub-optimal view angles.

(a)

(b)

Figure 4.10: If the fracture parts of the volume data is detected (marked as red in the figures), this salient view point selection algorithm can find the views that capture most amount of fracture area (as shown above)

Chapter 5

Conclusion

The Cranio-maxillofacial surgery is a very complex surgery. Computer aided pre-operative planning is needed for a successful CMF surgery. The design of a surgical simulation systems involves medical image segmentation, image registration and 3D model deformation.

The head is the most distinguishing part between people. The CMF surgeries aim to change the out appearance of the CMF region by surgical operations on the head anatomy. The CMF region is composed of rigid objects (bones) and deformable objects (muscles and skin etc.). The deformation of the deformable objects is the main task of many surgical simulation systems.

Many surgical simulation systems have been designed in the last two decades. They can be divided into reactive systems, predictive systems and automated planning systems. Their pros, cons and applications are discussed in detail. The reactive systems are mostly used for medical training and pre-operative planning of simple operations; the predictive systems are used for pre-operative planning of complex operations; the automated planning systems, which has great research potency, are used to assist the surgeons in making some difficult decisions or to offer the candidate surgical schedule for surgeons. In addition, the deformation methods that can be used in surgical simulation systems can be categorized into mass spring systems (MSM), finite element methods (FEM) and differential geometry methods (DG). The MSM is simple but inaccurate; the FEM is accurate but inefficient; if properly designed, the DG method can be both accurate and efficient.

After the literature review, we found some possible research topics in CMF surgical simulation. First, there is a strong demand for CMF automated planning systems. Second,

a proper DG algorithm for facial tissue deformation which is both accurate and efficient is also needed.

To start this research, we have done some preliminary work. First, a thresholding segmentation algorithm to segment the bone structure from the CT images is present. A good threshold is found experimentally. In addition, a salient view determination algorithm is designed to find the view which reveals the most amount of information from the data. Instead of the default views, which are often too bad, a salient view can give the surgeon better idea about the anatomy and the illness of the patient. All these works can contribute to the surgical simulation system that we want to come out finally.

Bibliography

[1] A. Alkhalifah, R. McGrindle, and V.N. Alexandrov. Immersive open surgery simulation. In *International Conference on Computational Science*, 2006.

[2] G. Bianchi, M. Harders, and G. Szekely. Mesh topology identification for mass-spring models. In *MICCAI*, 2003.

[3] D. Bielser and M.Gross. Open surgery simulation. In *Medicine Meets Virtual Reality*, 2002.

[4] Children's Hospital Boston. Skin anatomy and conditions. http://www.childrenshospital.org/az/Site784/mainpageS784P0.html, 2009.

[5] Mario Botsch and Olga Sorkine. On linear variational surface deformation methods. In *IEEE Transactions on Visualization and Computer Graphics*, 2008.

[6] H. Bourquain, A. Schenk, F.Link, B.Preim, G.Prause, and H.O. Peitgen. Hepavision2 - a software assistant for preoperative planning in living-related liver transplantation and oncologic liver surgery. In *Computer Assisted Radiology and Surgery*, 2002.

[7] Joel Brown, Stephen Sorkin, C. Bruyns, J.C. Latombe, and K. Montgomery M. Stephanides. Real-time simulation of deformable objects: tools and application. In *Computer Animation*, 2001.

[8] M.A.P. Castaneda and F.A. Cosio. Deformable model of the prostate for TURP sugery simulation. In *SIGGRAPH*, 2004.

[9] M. Chabanas, C. Marecaux, Y. Payan, and F.Boutault. Models for planning and simulation in computer assisted orthognatic surgery. In *MICCAI*, 2002.

[10] M. Chabanas and Y. Payan. A 3D finite element model of the face for simulation in plastic and maxill facial surgery. In *MICCAI*, 2000.

[11] K.S. Choi. Intractive cutting of deformable objects using force propagation approach and digital design analogy. In *SIGGRAPH*, 2006.

[12] E. Coste-Maniere, L. Adhami, F. Mourgues, and A. Carpentier. Planning, simulation, and augmented reality for robotic cardiac procedures: the stars system of the chir team. In *Seminars in Thoracic and Cardiovascular Surgery*, 2003.

[13] S. Cotin, H. Delingette, and N. Ayache. A hybrid elastic model for real-time cutting, deformations and force feedback for surgery training and simulation. In *Visual Computer*, 2000.

[14] J.R. Crouch, J.C. Merriam, and E.R. Crouch. Finite element model of cornea deformation. In *MICCAI*, 2005.

[15] F.B. de Casson and C. Laugier. Modeling the dynamics of a human liver for a minimally invasive surgery simulator. In *MICCAI*, 1999.

[16] F. Ding, W. Yang, W. K. Leow, and S. Venkatesh. Segmentation of soft organs by flipping-free mesh deformation. In *IEEE Workshop on Applications of Compuer Vision*, 2009.

[17] Feng Ding, Hao Li, Yuan Cheng, and Wee Kheng Leow. Medical volume image summarization. In *IEEE Workshop on Applications of Computer Vision*, 2009.

[18] M.P. do Carmo. Differential geometry of curves and surfaces. In *Prentice Hall*, 1976.

[19] J. Dutreuil, F. Goulette, C. Laurgeau, J.C. Zoreda, and S. Lundgren. Computer assisted dental implantology: A new method and a clinical validation. In *MICCAI*, 2001.

[20] E.Gladilin, A. Ivanov, and V. Roginsky. Generic approach for biomechanical simulation of typical boundary value problems in cranio-maxillofacial surger planning. In *MICCAI*, 2004.

[21] M.A. Elhelw, M.S. Atkins, M. Nicolaou, A. Chung, and G.Z. Yang. Photo-realistic tissue reflectance modelling for minimally invasive surgical simulations. In *MICCAI*, 2005.

[22] C.C. Galanis, M.M. Sfantsikopoulos, P.T. Koidis, N.M. Kafantaris, and P.G. Mpikos. Computer methods for automating preoperative dental implant planning: Implant positioning and size assignment. In *Computer Methods and Programs in Biomedicine*, 2007.

[23] G. Gelniker and D.Gossard. Deformable curve and surface finite-elements for free-form shape design. In *SIGGRAPH*, 1991.

[24] E. Gladilin, S. Zachow, P. Deuflhar, and H.C. Hege. Adaptive nonlinear elastic fem for realstic prediction of soft tissue in craniofacial surgery simulations. In *SPIE Medical Imaging Conference*, 2002.

[25] E. Gladilin, S. Zachow, P. Deuflhard, and H.C. Hege. Realistic prediction of individual facial emotion expressions for craniofacial surgery simulations. In *Visualizatoin, Image-Guided Procedures, and Display*, 2003.

[26] O. Goksel, S.E. Salcudean, S.P. Dimaio, R. Rohling, and J. Morris. 3D needle-tissue interaction simulation for prostate brachytherapy. In *Computer Aided Surgery*, 2005.

[27] E. Grinspun. A discrete model of thin shells. In *SIGGRAPH*, 2006.

[28] M. Hauth, O. Eszmuss, and W. Strasser. Analysis of numerical methods for the simulation of deformable models. In *The Visual Computer*, 2003.

[29] National University Hospital. Craniomaxillofacial surgery group, 2010. [Online; accessed 10-Jan-2010].

[30] H.C. Howland, R.H. Rand, and S.R Rubkin. A thin-shell model of the cornea and its application to corneal surgery. In *Refractive and Corneal Surgery*, 1991.

[31] E. Keeve, S. Girod, R.Kikinis, and B. Girod. Deformable modeling of facial tissue for craniofacial surgery simulation. In *Computer Aided Surgery*, 1998.

[32] Erwin Keeve, Sabine Girod, Arno Augustin, Andreas Binner, and Bernd Girod. Interactive craniofacial surgery simulation. In *ACM SIGGRAPH*, 1996.

[33] T. Kerwin, Hanwei Shen, and D. Stredney. Enhancing realism of wet surfaces in temporal bone surgical simulation. 2009.

[34] A. Kimura, J.J. Camp, R.A. Robb, and B.Davos. A prostate brachytherapy training rehearsal system - simulation of deromable needle insertion. In *MICCAI*, 2002.

[35] RR. Koch, S. Roth, M. Gross, A. Zimmermann, and H. Sailer. A framework for facial surgery simulation. In *Spring Conference on Computer Graphics*, 2002.

[36] Gulseren Kokten, Huseyin Balcioglu, and Mete Buyukertan. Supernumerary fourth and fifth molars: A report of two cases. In *Journal of Comteporary Dental Practice*, 2003.

[37] U. Kuhnapfel, H. Cakmak, and H. MaaB. Endoscopic surgery training using virtual reality and deformable tissue simulation. In *SIGGRAPH*, 2000.

[38] H. Li and W.K. Leow. Predictive surgical simulation for cardiac surgery. In *National University of Singapore*, 2008.

[39] H. Li, W.K. Leow, and I.S. Chiu. Predictive simulation of bidirectional Glenn shunt using a bybrid blood vessel model. In *MICCAI*, 2009.

[40] H. Li, Y. Qi W.K. Leow, and I.S. Chiu. Predictive surgical simulation of aorta reconstruction in cardiac surgery. In *MMVR*, 2009.

[41] L.L. Lian and Y.H. Chen. Haptic surgical simulation: An application to virtual suture. In *Computer-Aided Design and Application*, 2006.

[42] LittleBabyFaceFoundation. Facial deformities. http://www.littlebabyface.org, 2010.

[43] William E. Lorensen and Harvey E. Cline. Marching cubes: A high resolution 3d surface construction algorithm. In *SIGGRAPH*, 1987.

[44] Riidiger Marmulla and Herbert Niederdellmann. Computer-assisted bone segment navigation. In *Journal of Cranio-Maxillofacial Suigery*, 1998.

[45] H. Masuda, Y.Yoshioka, and Y. Furukawa. Interactive mesh deformation using equality-constrained least squares. In *SIGGRAPH*, 2006.

[46] H.P. Meinzer, M.Thron, and C.Cardenas. Computerized planning ofr liver surgery: an overview. In *SIGGRAPH*, 2002.

[47] MeshLab. Meshlab. http://meshlab.sourceforge.net/, 2010.

[48] W. Mollemans, F. Schutyse, J.V. Cleynenbreugel, and P. Suetens. Tetrahedral mass spring model for fast soft tissue deformation. In *Lecture Notes in Computer Science*, 2003.

[49] W. Mollemans, F. Schutyser, J.V. Cleynenbreugel, and P.Suetens. Fast foft tissue deformation with tetraheral mass spring model for maxillofacial surgery planning systems. In *MICCAI*, 2004.

[50] J. Mosegaard. LR-spring mass model for cardiac surgical simulation. In *Medicine Meets Virtual Reality*, 2004.

[51] J. Mosegaard, P. Herborg, and T.S. Sorensen. A GPU accelerated spring mass system for surgical simulation. In *Medicine Meets Virtual Reality*, 2005.

[52] M.Rieger, M.Gabl, H. Gruber, W.R. Jaschkel, and A. Mallouhi. CT virtual reality in the preoperative workup of malunited distal radius fractures: preliminary results. In *European Radiology*, 2004.

[53] A. Nealen, M. Muller, R. Keiser, E. Boxermann, and M. Carlson. Physically based deformable models in computer graphics. In *Eurographics, State of Art Reports*, 2005.

[54] H.W. Nienhuys and A.F. van der Stappen. A surgery simulation supporting cuts and finite element deformation. In *MICCAI*, 2001.

[55] H.W. Nienhuys and A.F. van der Stappen. A delaunay approach to interactive cutting in triangulated surfaces. In *International Workshop on Algorithmic Foundations of Robotics*, 2003.

[56] International Encyclopedia of Science. skeletal muscles and muscle groups, 2010. [Online; accessed 10-Jan-2010].

[57] Dinesh K. Pai. Strands: Interactive simulation of thin solids using cosserat models. In *EUROGRAPHICS*, 2002.

[58] ParaView. Paraview. http://www.paraview.org/, 2010.

[59] S. Park, X. Gou, H. Shin, and H. Qin. Surface completion for shape and appearance. In *The Vision Computer*, 2006.

[60] D. Richens, M. Fielda, S. Hashima, M. Nealeb, and C. Oakley. A finite element model of blunt traumatic aortic rupture. In *European Journal of Cardio-Thoracic Surgery*, 2004.

[61] R. Sierra, J. Zatonyi, M. Bajka, G. Szekely, and M. Harders. hydrometra simulation for vr-based hysteroscopy training. In *MICCAI*, 2005.

[62] T.S. Sorensen and J. Mosegaard. Virtual open heart surgery: training complex surgical procedures in congenital heart desease. In *ACM SIGGRAPH*, 2006.

[63] T.S. Sorensen, J. Stawiaski, and J. Mosegaard. Virtual open heart surgery: obtaining models suitable for surgical simulation. In *Medicine Meets Virtual Reality*, 2007.

[64] P. Tardieu, L. vrielinck, E.Escolano, M. Henne, and A.L. Tardieu. Computer-assisted implant placement: scan template, SimPlant,SurgiGuide, and SAFE system. In *International Journal of Preiodotics and Restorative Dentistry*, 2007.

[65] D. Terzopoulos, J. Platt, A. Barr, and K. Fleischer. Elastically deformable models. In *SIGGRAPH*, 1987.

[66] M. Teschner, s. Girod, and B. Girod. Optimization approaches for soft-tissue prediction in craniofacial surgery simulation. In *MICCAI*, 1999.

[67] M.J. Troulis, P.Everett, E.B. Seldin, R. Kikinis, and L.B. Kaban. Development of a three-dimesional treatment planning system based on computed tomographic data. In *Journal of Oral Maxillofacial Surgery*, 2002.

[68] C.Y. Tso, R.R. Ellis, J. Rudan, and M.M Harrison. A surgical planning and guidance system for high tibial osteotomies. In *MICCAI*, 1998.

[69] K. Verstreken, J. van Cleynenbreugel, G.Marchal, D. van Steenberghe, and P. Suetens. Computer-assisted planning of oral implantsurgery - an approach using virtual reality. In *Medicine Meets Virtual Reality*.

[70] R.W. Webster, D.I. Zimmerman, B.J. Mohler, M.G. Melkonian, and H.R.S. A prototype haptic suturing simulator. In *Stud Health Tecgbik Inform*, 2001.

[71] W. Welch and A. Witkin. Variational surface modelling. In *SIGGRAPH*, 1992.

[72] Y. Weng, W. Xu, Y. Wu, K. Zhou, and B. Guo. 2D shape deformation using nonlinear least squares optimization. In *Visual Computer*, 2006.

[73] Marcin Wierzbicki, Maria Drangova, Gerard Guiraudon, and Terry Peters. Validation of dynamic heart models obtained using non-linear registration for virtual reality training, planning, and guidance of minimally invasive cardiac surgeries. In *Medical Image Analysis*, 2004.

[74] Wikipedia. Human skull. http://en.wikipedia.org/wiki/Skull, 2009.

[75] Wikipedia. Cleft lip and palate, 2010. [Online; accessed 10-Jan-2010].

[76] Wikipedia. Traffic collision, 2010. [Online; accessed 10-Jan-2010].

[77] Wikipedia. Trevor rees-jones. http://en.wikipedia.org/wiki/TrevorRees-Jones, 2010.

[78] J.R. Wollmuth, D.R. Bree, B.P. Cupps, M.F. Krock, B.J. Pomerantz, R.P. Pasquea, A. Howells, N.Moazami, N.T. Kouchoukos, and M.K. Pasque. Left ventricular wall stress in patients with severe aortic insufficiency with finite element analysis. In *The Annuals of Thoracic Surgery*, 2006.

[79] WrongDiagnosis. statistics by country for cleft palate. http://WrongDiagnosis.com/, 2010.

[80] X. Wu, M.S. Downes, T. Goketekin, and F. Tendick. Adaptive nonlinear finite elements for deformable body simulation using dynamic progressive meshes. In *Eurographics*, 2001.